Inorg. Chem. **2008**, *47*, 8405−8411

Electron-Transfer Reactions of Nitrosyl and Superoxo Metal Complexes

Wenjing Song, Arkady Ellern, and Andreja Bakac*

Chemistry Department, Iowa State University, Ames, Iowa 50011

Received May 13, 2008

Novel chromium nitrosyl complexes $L(H_2O)CrNO^{2+}$ ($L = L^1$ = 1,4,8,11-tetraazacyclotetradecane, L^2 = *meso*-Me_6-1,4,8,11-tetraazacyclotetradecane) are oxidized by $Ru(bpy)_3^{3+}$ to $LCr(H_2O)_2^{3+}$ and NO with rate constants k = 2.22 M^{-1} s^{-1} (L^1) and 6.83 (L^2). Analogous reactions of the superoxo complexes $L(H_2O)CrOO^{2+}$ are only slightly faster, k = 45 M^{-1} s^{-1} (L^1) and 15 M^{-1} s^{-1} (L^2). A related rhodium complex $L^2(H_2O)RhOO^{2+}$ has k = 15.8 M^{-1} s^{-1}. These results, combined with our earlier data for the oxidation of $Cr_{aq}NO^{2+}$ and $Cr_{aq}OO^{2+}$, suggest only a modest role for thermodynamics in determining the kinetics of oxidation. This behavior is even more pronounced in the oxidation of rhodium hydrido and hydroperoxo complexes, with the latter reacting more than 10^5-fold faster despite being thermodynamically less favored by more than 0.3 V. The X-ray crystal structure of $[L^1(H_2O)CrNO](ClO_4)_2$ supports the limiting $Cr^{III}-NO^-$ description for the complex cation.

Introduction

Nitrosyl and superoxo metal complexes are important intermediates in biological and catalytic processes. Typically, they are generated from NO or O_2 and a low-oxidation-state metal complex (eq 1).

$$LM^n + NO\ (\text{or}\ O_2) \rightleftarrows LMNO^n\ (\text{or}\ LMOO^n) \qquad (1)$$

The role of these and related species in various processes and the mechanism of their formation and disappearance are the focus of an intense area of research.[1−11] The most obvious mechanism for the release of NO/O_2 is the homolytic cleavage of the metal−NO/O_2 bond, i.e., the reverse of reaction 1. The dissociation can in some cases be accelerated by prior oxidation to raise the metal to an oxidation state with low affinity for NO/O_2. This mechanism, termed oxidative homolysis, was found to operate in the reactions of nitrosyl hemes with peroxynitrite and nitrogen dioxide.[12] Similarly, polypyridine complexes of ruthenium and iron were found to oxidize the abiological nitrosyl[13] and superoxo[14] complexes of aquachromium(III), $Cr_{aq}OO^{2+}$ and $Cr_{aq}NO^{2+}$ (eqs 2 and 3). The oxidation was accompanied by the loss of NO/O_2 at rates unprecedented for substitution at chromium(III). In fact, the oxidized intermediates were never observed, so that the concerted oxidation and O_2/NO loss, i.e., dissociative electron transfer, cannot be ruled out.

$$Ru(bpy)_3^{3+} + Cr_{aq}NO^{2+} \rightarrow Ru(bpy)_3^{2+} + Cr_{aq}^{3+} + NO \quad k_{MNO} \qquad (2)$$

$$Ru(bpy)_3^{3+} + Cr_{aq}OO^{2+} \rightarrow Ru(bpy)_3^{2+} + Cr_{aq}^{3+} + O_2 \quad k_{MOO} \qquad (3)$$

In that earlier work, a strong correlation was observed between the kinetics and the reduction potential of the

* To whom correspondence should be addressed. E-mail: bakac@ameslab.gov.

(1) *Nitric Oxide. Biology and Pathobiology*; Ignarro, L. J., Ed.; Academic: San Diego, 2000.
(2) Averill, B. A. *Chem. Rev.* **1996**, *96*, 2951–2964.
(3) Ford, P. C.; Lorkovic, I. M. *Chem. Rev.* **2002**, *102*, 993–1017.
(4) Hayton, T. W.; Legzdins, P.; Sharp, W. B. *Chem. Rev.* **2002**, *102*, 935–991.
(5) Activation of O_2 and Homogeneous Catalytic Oxidation; Barton, D. H. R., Martell, A. E., Sawyer, D. T., Eds.; Plenum: New York, 1993.
(6) Wong, C.-L.; Switzer, J. A.; Balakrishnan, K. P.; Endicott, J. F. *J. Am. Chem. Soc.* **1980**, *102*, 5511–5518.
(7) *Advances in Catalytic Activation of Dioxygen by Metal Complexes*; Simandi, L. I., Ed.; Kluwer: Dordrecht, The Netherlands, 2003; Vol. *26*.
(8) *Biomimetic Oxidations Catalyzed by Transition Metal Complexes*; Meunier, B., Ed.; Imperial College Press: London, 2000.
(9) Shilov, A. E.; Shul'pin, G. B. *Activation and Catalytic Reactions of Saturated Hydrocarbons in the Presence of Metal Complexes*; Kluwer: Dordrecht/Boston/London, 2000; Chapters 9−11.
(10) Taki, M.; Teramae, S.; Nagatomo, S.; Tachi, Y.; Kitagawa, T.; Itoh, S.; Fukuzumi, S. *J. Am. Chem. Soc.* **2002**, *124*, 6367–6377.
(11) Kim, E.; Chufan, E. E.; Kamaraj, K.; Karlin, K. *Chem. Rev.* **2004**, *104*, 1077–1133.
(12) Herold, S.; Boccini, F. *Inorg. Chem.* **2006**, *45*, 6933–6943.
(13) Song, W.; Bakac, A. *Chem.−Eur. J.* **2008**, *14*, 4906–4912.
(14) Bakac, A.; Espenson, J. H.; Janni, J. A. *J. Chem. Soc., Chem. Commun.* **1994**, 315.

10.1021/ic800867j CCC: $40.75
Published on Web 08/12/2008

oxidants, consistent with an outer-sphere electron-transfer process.[13] We have now extended these studies in two directions. First, we examined the oxidation of several macrocyclic superoxo and nitrosyl complexes of chromium and rhodium to determine how this wider selection of metals and ligands will influence the reactivity pattern established for the aquachromium complexes $Cr_{aq}OO^{2+}$ and $Cr_{aq}NO^{2+}$.

Second, we studied the oxidation of macrocyclic rhodium(III) hydroperoxo and hydrido complexes, $L^2(H_2O)RhOOH^{2+}$ and $L^2(H_2O)RhH^{2+}$, which together with $L^2(H_2O)RhOO^{2+}$ form a series having different reactive groups in a constant metal−ligand environment. It is rare, although not unprecedented,[15−17] that the same metal−ligand combination will stabilize intermediates formed by the activation of both oxygen and hydrogen. This series provides an opportunity to look at the reactivity of different groups, to attempt to build the connection between the kinetics and thermodynamics, and to provide more insight into the process of activation of oxygen, hydrogen, and perhaps other small molecules by transition-metal catalysts.

In our earlier study of hydrogen atom abstraction (HAT) by superoxo complexes and nitroxyl free radicals,[18] the hydrides and hydroperoxides exhibited similar kinetics despite the great thermodynamic advantage of the hydrides. Comparison with other substrates suggested that the reactivity of hydroperoxides was "normal" and that of the hydrides was unusually low. Although steric effects clearly played a role in some cases, they did not appear sufficient to explain the low reactivity of the hydrides. None the less, determining the kinetics of oxidation of $L^2(H_2O)RhH^{2+}$ and $L^2(H_2O)RhOOH^{2+}$ in an outer-sphere process, where steric effects should play a minimal role, did provide additional impetus for this work and an opportunity to get a better estimate of the difference in intrinsic reactivities of the two.

The structures of the metal superoxo complexes with macrocyclic ligands L^1 (1,4,8,11-tetraazacyclotetradecane) and L^2 (*meso*-Me_6-1,4,8,11-tetraazacyclotetradecane) are shown below where M = Cr^{III} or Rh^{III}.

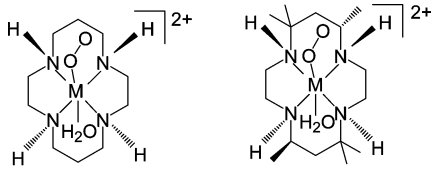

$L^1(H_2O)M^{III}OO^{2+}$ $L^2(H_2O)M^{III}OO^{2+}$

Experimental Section

Aqueous solutions of the superoxo, hydroperoxo, and hydrido metal complexes were prepared by our previously published procedures.[18] Solid $[(salen)Cr^{V}O](CF_3SO_3)$ was prepared as previously described.[19] Solutions of $L(H_2O)CrNO^{2+}$ (L = L^1, L^2) were prepared by bubbling NO through acidic solutions of $LCr(H_2O)_2^{2+}$ and purified by ion exchange on a Sephadex C-25. The concentration of chromium was determined by inductively coupled plasma mass spectrometry (ICP-MS). Gaseous NO (Matheson) was purified by passage through Ascarite, sodium hydroxide, and water.[13] Stock solutions of NO were prepared by bubbling the purified gas through argon-saturated 0.10 or 0.01 M $HClO_4$ for 30 min. Solutions of $LCr(H_2O)_2^{2+}$ were generated by a zinc amalgam reduction of $LCr(H_2O)_2^{3+}$. Solutions of $Ru(bpy)_3^{3+}$ were generated photochemically from $Ru(bpy)_3^{2+}$ and excess $(NH_3)_5Co(H_2O)^{3+}$ (2 mM).[13] Kinetic experiments typically utilized small concentrations of $Ru(bpy)_3^{3+}$ and a large excess of the reductant. All of the concentrations were varied as much as was experimentally feasible. Whenever possible, the conditions were reversed so that $Ru(bpy)_3^{3+}$ was in excess. Because of the slow autoreduction of $Ru(bpy)_3^{3+}$ under our experimental conditions, some of the kinetic data had to be corrected for this parallel loss of $Ru(bpy)_3^{3+}$, especially when the latter was in excess. The correction was always small and best approximated with a linear term; see the Results section. The reaction of $(salen)Cr^{V}O^{+}$ with $L^2(H_2O)RhOOH^{2+}$ was examined briefly under second-order conditions, with the two reagents present in approximately equimolar concentrations (0.027−0.080 mM) in 5−30 mM $HClO_4$ at variable ionic strength. The kinetics were monitored at 600 nm, where $(salen)Cr^{V}O^{+}$ exhibits a maximum (ϵ = 2400 M^{-1} cm^{-1}).

A Shimadzu 3101 PC spectrophotometer was used for kinetic and UV−visible spectral measurements. An Applied Photophysics stopped-flow spectrophotometer was used for fast reactions. All of the kinetic data were collected at 25.0 ± 0.2 °C. Data analyses were done with KaleidaGraph 3.6 PC software, and simulations with the Kinsim/Fitsim52 for PC.

Elemental analysis was carried out on a slightly moist sample of $L^1(H_2O)CrNO(ClO_4)_2$ obtained by evaporating an acidic ($HClO_4$) aqueous solution of the complex. Drying the perchlorate salt at higher temperatures was not considered safe, and prolonged exposure to a vacuum appeared to deteriorate the compound. The experimental C, H, and N data (C, 19.99; H, 4.42; N, 11.44) require a molecule of $HClO_4$ of crystallization per cation, i.e., $C_{10}H_{24}Cl_2CrN_5O_{10}$, $HClO_4$ (calcd: C, 20.10; H, 4.22; N, 11.72). The N/C ratio (0.57) confirms that the molecule contains five nitrogen atoms per molecule (calculated N/C = 0.58).

Crystal Structure Determination. Slow evaporation of solutions of $L^1(H_2O)CrNO^{2+}$ in 0.2 M $HClO_4$ and of $L^2(H_2O)CrNO^{2+}$ in 0.2 M CF_3SO_3H yielded green crystalline solids. The crystals for structure determination were selected under a layer of solvent under ambient conditions, covered with epoxy glue, and mounted and centered in the X-ray beam with the aid of a video camera. The crystal evaluation and data collection were performed at 173 K with a Bruker CCD-1000 diffractometer with Mo Kα (λ = 0.710 73 Å) radiation and a detector-to-crystal distance of 5.03 cm.

The initial cell constants were obtained from three series of ω scans at different starting angles. Each series consisted of 30 frames collected at intervals of 0.3° in a 10° range about ω. The reflections were successfully indexed by an automated indexing built-in routine. The final cell constants were calculated from a set of strong reflections from the actual data collection that used the full sphere routine. Four sets of frames were collected with 0.3° scans in ω. The data sets were corrected for Lorentz and polarization effects. The absorption correction was based on a fit of a spherical harmonic function to the empirical transmission surface as sampled by multiple equivalent measurements.[20] All further calculations were

(15) Bakac, A. *Coord. Chem. Rev.* **2006**, *250*, 2046–2058.
(16) Roberts, H. L.; Symes, W. R. *J. Chem. Soc. A* **1968**, 1450–1453.
(17) Mirza, S. A.; Bocquet, B.; Robyr, C.; Thomi, S.; Williams, A. F. *Inorg. Chem.* **1996**, *35*, 1332–1337.
(18) Vasbinder, M.; Bakac, A *Inorg. Chem.* **2007**, *46*, 2921–2928.
(19) Bakac, A.; Guzei, I. A. *Inorg. Chem.* **2000**, *39*, 736–740.
(20) Blessing, R. H. *Acta Crystallogr.* **1995**, *A51*, 33–38.

Table 1. Crystallographic Data for $[([14]aneN_4)(H_2O)CrNO]^{2+}\cdot H_2O$ (**1**) and [*meso*-Me_6-$([14]aneN_4)(H_2O)CrNO](CF_3SO_3)_2$ (**2**)

empirical formula	$C_{10}H_{28}Cl_2CrN_5O_{11}$ (**1**)	$C_{18}H_{38}CrF_6N_5O_8S_2$ (**2**)
fw	517.27	682.65
temperature (K)	173(2)	173(2)
wavelength (Å)	0.710 73	0.710 73
cryst syst	monoclinic	triclinic
space group	$P2(1)/n$	$P\bar{1}$
unit cell dimens	$a = 14.783(3)$ Å	$a = 8.738(2)$ Å
	$b = 8.7349(18)$ Å	$b = 8.959(2)$ Å
	$c = 16.814(3)$ Å	$c = 10.557(2)$ Å
	$\beta = 105.186(3)°$	$\alpha = 95.414(4)°$
		$\beta = 105.380(4)°$
		$\gamma = 110.034(4)°$
volume (Å^3)	2095.3(7)	732.8(3)
Z	4	1
density (calcd) (Mg m^{-3})	1.640	1.547
abs coeff (mm^{-1})	0.864	0.620
$F(000)$	1076	355
cryst size (mm^3)	0.35 × 0.31 × 0.28	0.30 × 0.30 × 0.08
reflns collected	18 424	5446
indep reflns	4959 [R(int) = 0.0343]	2490 [R(int) = 0.0229]
max and min transmn	1 and 0.89	1 and 0.74
data/restraints/param	4959/3/290	2490/19/269
GOF on F^2	1.056	0.987
final R indices [$I > 2\sigma(I)$][a]	R1 = 0.0536, wR2 = 0.1432	R1 = 0.0556, wR2 = 0.1557
R indices (all data)[a]	R1 = 0.0618, wR2 = 0.1510	R1 = 0.0701, wR2 = 0.1686
largest diff peak and hole (e Å^{-3})	+1.301 and −0.887	+0.370 and −0.322

[a] $R1 = \sum ||F_o| - |F_c||/\sum|F_o|$ and $wR2 = \{\sum[w(F_o^2 - F_c^2)^2]\sum[w(F_o^2)^2]\}^{1/2}$.

performed with the *SHELXTL* software package.[21] The structure was solved by direct methods. The positions of almost all non-hydrogen atoms were found by direct methods. The remaining atoms were located in an alternating series of least-squares cycles and difference Fourier maps.

***trans*-$[L^1(H_2O)CrNO](ClO_4)_2\cdot H_2O$.** The data were harvested with an exposure time of 10 s frame^{-1}. The systematic absences in the diffraction data were consistent with the space group $P2_1/n$ and yielded chemically reasonable and computationally stable results. All non-hydrogen atoms were refined in the full-matrix anisotropic approximation. Hydrogen atoms of coordinated and solvent water were found in a difference Fourier map, and their positions were constrained. All hydrogen atoms including ligated and solvent water were found objectively in a Fourier map. Their positions were constrained, and atoms were allowed to ride on the neighboring atoms with relative isotropic displacement coefficients. One cluster molecule and one solvent water molecule were found in the asymmetric unit of a primitive monoclinic cell.

***trans*-$[L^2(H_2O)CrNO](CF_3SO_3)_2$.** The data were harvested with an exposure time of 40 s frame^{-1}. The systematic absences in the diffraction data were consistent for the space groups $P1$ and $P\bar{1}$[2]. The E statistics suggested the noncentrosymmetric space group $P1$. The refinement indicated the existence of a racemic twin, which is highly unlikely. The analysis of coordinates also indicated the existence of an inversion center, and all further calculations were performed in a more realistic $P\bar{1}$ space group after standard transformation of coordinates to satisfy this symmetry. A counterion, half of the centrosymmetric cation (with chromium atom at the inversion center), and disordered NO and H_2O in axial positions of the typical octahedral coordination around chromium were found in the asymmetric unit of the triclinic cell. All attempts to use the disorder model with overlapped separated positions for axial groups failed. Thus, it is not possible to discuss bond lengths and angles for axial ligands. The triflate counterion is disordered by two positions with occupancy factors of about 0.5. All non-hydrogen atoms were refined in the full-matrix anisotropic approximation. All hydrogen atoms were placed in the structure factor calculation at idealized positions and were allowed to ride on the neighboring atoms with relative isotropic displacement coefficients. The X-ray analysis shows that the chromium coordination in this complex is very similar to that observed in *trans*-$[L^1(H_2O)CrNO](ClO_4)_2\cdot H_2O$. However, the chromium atom is at an inversion center, forcing the $Cr-N_4$ entity into a perfectly flat geometry.

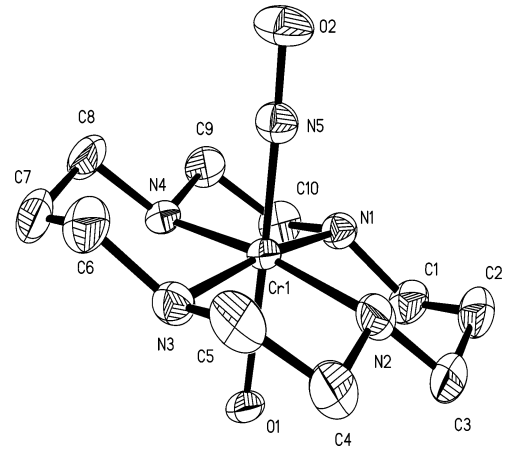

Figure 1. ORTEP drawing of $[L^1(H_2O)CrNO](ClO_4)_2$ at the 50% probability level. Bond distances/Å: Cr1−N1, 2.072(2); Cr1−N2, 2.073(3); Cr1−N3, 2.061(2); Cr1−N4, 2.061(3); Cr1−N5, 1.686(2); Cr1−O1, 2.102(2); N5−O2, 1.186(3). Bond angles/deg: N5−Cr1−N4, 93.53(12); N5−Cr1−N3, 94.23(11); N5−Cr1−N1, 93.71(11); N5−Cr1−N2, 93.75(12); N5−Cr1−O1, 177.90(11).

Crystallographic data and the molecular structures of $L^1(H_2O)CrNO^{2+}$ and $L^2(H_2O)CrNO^{2+}$ are shown in Table 1 and Figures 1 and 2. Complete crystallographic data have been deposited with the Cambridge Structural Database under reference numbers 667856 and 667857. These data can be obtained free of charge at www.ccdc.cam.uk/data_request/cif.

Results

Molecular structure of $L^1(H_2O)CrNO^{2+}$ is shown in Figure 1. The four equatorial nitrogen atoms are coplanar (rms 0.006). The chromium atom is displaced from the N_4 plane

(21) Sheldrick, G. M. *Acta Crystallogr.* **2008**, *A64*, 112–122.

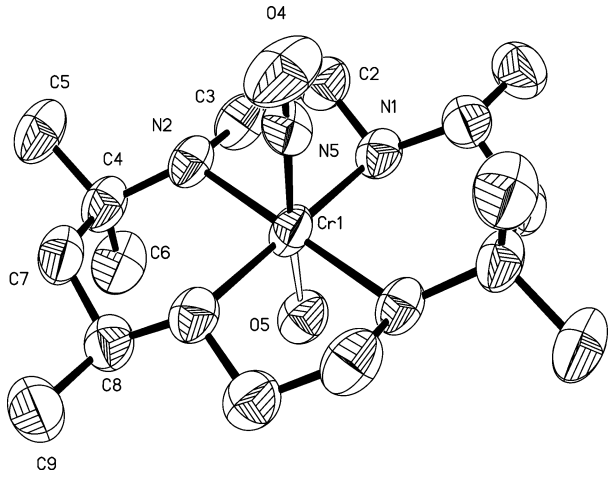

Figure 2. ORTEP drawing of $[L^2(H_2O)CrNO]^{2+}$ at the 30% probability level with hydrogen atoms omitted. For clarity, only one of the two disordered configurations of axial ligands is shown. Selected geometrical parameters: Cr1−N1, 2.064(3) Å; Cr1−N2, 2.096(3) Å; O4−N5−Cr1 174.3(4)°.

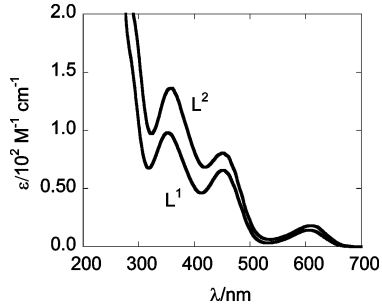

Figure 3. Electronic absorption spectra of $L(H_2O)CrNO^{2+}$ complexes. Bottom: L = L^1. Top: L = L^2.

by 0.137(1) Å toward NO. The Cr−N−O entity is almost linear, 178.40(13)°, and the axial Cr−N5 distance [1.686(2) Å] is much shorter than the average equatorial Cr−N bond length (2.067 Å), consistent with multiple bonding between chromium and NO. The Cr−O1 bond trans to NO is long (2.102 Å) compared to Cr−O distances in similar complexes in the absence of NO or other trans-labilizing ligands. For example, the Cr^{III}−O distance is 2.008(4) Å in *trans*-$[L^2Cr(H_2O)_2](ClO_4)_3\cdot 4H_2O$,[22] 1.984(2) Å in *trans*-$[L^1Cr(OH)(H_2O)](CF_3SO_3)_2$,[23] 1.945(3) Å in *trans*-$[L^1Cr(OH)_2]ClO_4$,[23] and 1.977(3) and 1.988(3) Å in *trans*-$[L^1Cr(OH)(H_2O)]Br_2,H_2O$.[24] The Cr−*trans*-$H_2O$ distance in the macrocyclic $L^1(H_2O)CrNO^{2+}$ is even greater than that in $Cr_{aq}NO^{2+}$, 2.057(2) Å,[25] strongly supporting the $Cr^{III}NO^-$ limiting structure.

UV−visible spectra of $L(H_2O)CrNO^{2+}$ (L = L^1, L^2) are shown in Figure 3. The maxima for the L^1 complex are at 603 nm (ϵ = 14.2 M^{-1} cm^{-1}), 451 nm (65.9 M^{-1} cm^{-1}), and 353 nm (98.1 M^{-1} cm^{-1}), and those for $L^2(H_2O)CrNO^{2+}$, at 610 nm (ϵ = 18.0 M^{-1} cm^{-1}), 452 nm (80.7 M^{-1} cm^{-1}), and 358 nm (136 M^{-1} cm^{-1}).

Table 2. Rate Constants (M^{-1} s^{-1}) for Reactions of $Ru(bpy)_3^{3+}$ with $L(H_2O)MX^{2+}$ Complexes of Rhodium and Chromium[a]

	X =				
LM	O_2[b]	NO[c]	H	OOH	k_{MO2}/k_{MNO}
Cr_{aq}	2630[d]	142[e]			18
L^1Cr	45.0	2.22[f]			20
L^2Cr	15.0	6.83[f]			2
L^2Rh	15.8		<0.2	4.74×10^4	

[a] Conditions: 25.0 °C, 1.0 M $HClO_4$. [b] k_{MOO}. [c] Value of k_2, obtained by correcting the experimental rate constant by an appropriate stoichiometric factor n; see the text. [d] Reference 14. [e] Reference 13. [f] $n = 3$.

Oxidation of $L(H_2O)CrNO^{2+}$ (L = L^1, L^2). The kinetics of oxidation of the nitrosyl complexes were studied under pseudo-first-order conditions with a large excess of $L(H_2O)CrNO^{2+}$ complexes over $Ru(bpy)_3^{3+}$. The absorbance at 452 nm, corresponding to the growth of $Ru(bpy)_3^{2+}$, increased exponentially. Pseudo-first-order rate constants in the $L^2(H_2O)CrNO^{2+}/Ru(bpy)_3^{3+}$ reaction exhibited a linear dependence on the concentration of the nitrosyl complexes with a slope of 20.9 ± 0.67 M^{-1} s^{-1} (Figure S1 in the Supporting Information). These rate constants represent the product nk_{MNO}, where the stoichiometric factor n is determined by the number of molecules of $Ru(bpy)_3^{3+}$ consumed per kinetic step of eq 2.

Under a reasonable assumption that the oxidation of $L^2(H_2O)CrNO^{2+}$ follows the general mechanism in eqs 2 and 4−7, as established earlier for the oxidation of $Cr_{aq}NO^{2+}$,[13] and using the known rate constants[13] for reactions 4−7, it can be easily shown that the chemistry in eq 7 is much slower than that in reactions 2 and 4−6. Consistent with this fact, our simulations of the reaction scheme in eqs 2 and 4−7 provided excellent agreement with experimental data for n = 3, resulting in k_{MNO} = 6.83 ± 0.16 M^{-1} s^{-1}. All of the rate constants are summarized in Table 2.

$$Ru(bpy)_3^{3+} + NO \rightarrow Ru(bpy)_3^{2+} + NO^+ \quad (4)$$

$$NO^+ + H_2O \rightleftarrows HNO_2 + H^+ \quad \text{fast} \quad (5)$$

$$Ru(bpy)_3^{3+} + HNO_2/NO_2^- \rightarrow Ru(bpy)_3^{2+} + NO_2 \quad (6)$$

$$2NO_2 \rightleftarrows N_2O_4 \xrightarrow{H_2O} NO_3^- + HNO_2 + H^+ \quad (7)$$

For the complex $L^1(H_2O)CrNO^{2+}$, the plot of k_{obs} against the concentration of $L^1(H_2O)CrNO^{2+}$ also yielded a linear plot but one that exhibited a small intercept (Figure S1 in the Supporting Information). The reason for this behavior is probably the small rate constant, which makes reaction 7 important at the lowest concentrations of the nitrosyl complex but not at the high end. As a result, the overall stoichiometry $[Ru(bpy)_3^{3+}]/[L^1(H_2O)CrNO^{2+}]$ decreases from >3 to 3 as $[L^1(H_2O)CrNO^{2+}]$ increases, yielding a curved plot, which, in the limited range of concentrations used, may appear as a straight line with an intercept. Simulations with Kinsim confirmed the expected change in the stoichiometry under the conditions in Figure S1 in the Supporting Information. The slope of the line in Figure S1 in the Supporting Information (6.66 ± 0.38 M^{-1} s^{-1}) and the stoichiometric

(22) Lemma, K.; Ellern, A.; Bakac, A. *Dalton Trans.* **2006**, 58–63.
(23) Goodson, P. A.; Glerup, J.; Hodgson, D. J.; Jensen, N. B.; Michelsen, K. *J. Chem. Soc., Dalton Trans.* **2001**, 2783–2790.
(24) Palmer, R. A.; Potter, B. S.; Tanriverdi, S.; Lisgarten, J. N.; Flint, C. D.; Gazi, D. M. *Acta Crystallogr., Sect. C* **1996**, *C52*, 1177–1180.
(25) Ardon, M.; Cohen, S. *Inorg. Chem.* **1993**, *32*, 3241–3243.

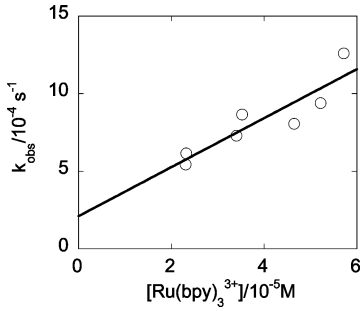

Figure 4. Plot of the pseudo-first-order rate constant vs the concentration of $Ru(bpy)_3^{3+}$ for the reaction with $L^2(H_2O)RhOO^{2+}$ (2−6 μM) in 1.0 M $HClO_4$.

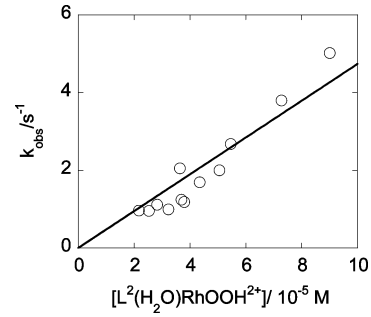

Figure 5. Plot of the pseudo-first-order rate constant vs the concentration of $L^2(H_2O)RhOOH^{2+}$ in 1.0 M $HClO_4$. $[Ru(bpy)_3^{3+}] = 4-8$ μM.

factor $n = 3$ were used to calculate the rate constant listed in Table 2, $k_{MNO} = 2.22 \pm 0.13$ M^{-1} s^{-1}.

Oxidation of $L(H_2O)MOO^{2+}$ (M = Cr, Rh; L = L^1, L^2). In the presence of a large excess of $L(H_2O)CrOO^{2+}$ complexes, the appearance of $Ru(bpy)_3^{2+}$ was exponential and yielded pseudo-first-order rate constants that showed a linear dependence on $[L(H_2O)CrOO^{2+}]$. The rate constants $k_{MOO} = 45.0 \pm 0.13$ M^{-1} s^{-1} (L = L^1) and 15.0 ± 0.06 M^{-1} s^{-1} (L = L^2) were obtained from the slopes of the k_{obs} vs $[L(H_2O)CrOO^{2+}]$ plots shown in Figure S2 in the Supporting Information.

The oxidation of the rhodium complex $L^2(H_2O)RhOO^{2+}$ with $Ru(bpy)_3^{3+}$ yielded exponential and reproducible traces only when $Ru(bpy)_3^{3+}$ was used in a large excess over the superoxo complex. Under reverse conditions (i.e., excess $L^2(H_2O)RhOO^{2+}$), data reproducibility and fits to the exponential rate equation were poor. We attributed this behavior to the presence of small and variable amounts of the hydroperoxo complex, $L^2(H_2O)RhOOH^{2+}$, in our solutions of the superoxo complex, which is typically prepared from $L^2Rh(H_2O)^{2+}$ and O_2. Small amounts of the hydroperoxo complex can be formed by the reduction of newly generated $L^2(H_2O)RhOO^{2+}$ with $L^2Rh(H_2O)^{2+}$ even in the presence of a large excess of O_2, because the reactions of $L^2Rh(H_2O)^{2+}$ with O_2 and with $L^2(H_2O)RhOO^{2+}$ are faster than mixing, which results in less than homogeneous distribution of the reactants during the preparation. The hydroperoxo complex reacts rapidly with $Ru(bpy)_3^{3+}$ (see below), affecting the $L^2(H_2O)RhOO^{2+}/Ru(bpy)_3^{3+}$ reaction the most when $Ru(bpy)_3^{3+}$ is limiting. This problem was not encountered in the oxidations of $L^2(H_2O)CrOO^{2+}$ because the corresponding hydroperoxide is highly unstable and short-lived.[22,26] The remainder of the experiments with $L^2(H_2O)RhOO^{2+}$ were run with excess $Ru(bpy)_3^{3+}$, which greatly improved the reproducibility. However, a slow background self-reduction of $Ru(bpy)_3^{3+}$ could not be completely avoided. The kinetic traces were fitted to an {exponential + linear} equation, with the linear term corresponding to $Ru(bpy)_3^{3+}$ decay. A plot of the pseudo-first-order rate constants against $[Ru(bpy)_3^{3+}]$ (Figure 4) is linear with a slope $k_{MOO} = 15.8 \pm 0.3$ M^{-1} s^{-1} and an intercept of $(2.1 \pm 1.4) \times 10^{-4}$ s^{-1}. The latter is in the correct range for Rh−O_2 homolysis, $k_h = (2.18 \pm 0.37) \times 10^{-4}$ s^{-1},[27] suggesting that the chemistry in eqs 8 and 9 provides an additional pathway for the loss of the superoxo complex, with the kinetics independent of the concentration of $Ru(bpy)_3^{3+}$. The rate constant k_9 for the oxidation of $L^2(H_2O)Rh^{2+}$ with $Ru(bpy)_3^{3+}$ is not available, but it must be large to compete with the reverse of eq 8 in O_2-saturated solutions. The large uncertainty associated with the value of the intercept prevents us from estimating k_9 from the data in Figure 4.

$$L^2(H_2O)RhOO^{2+} \rightleftarrows L^2(H_2O)Rh^{2+} + O_2 \quad (8)$$

$$Ru(bpy)_3^{3+} + L^2(H_2O)Rh^{2+} + H_2O \rightarrow Ru(bpy)_3^{2+} + L^2(H_2O)Rh^{3+} \quad (9)$$

Oxidation of $L^2(H_2O)RhOOH^{2+}$ and $L^2(H_2O)RhH^{2+}$. The reaction of $L^2(H_2O)RhOOH^{2+}$ and $Ru(bpy)_3^{3+}$ obeys a mixed second-order rate law with a rate constant $k = (4.74 \pm 0.26) \times 10^4$ M^{-1} s^{-1} (Figure 5).

The intense UV spectrum of the product $Ru(bpy)_3^{2+}$ obscures the 270 nm region, where the other expected product, $L^2(H_2O)RhOO^{2+}$ exhibits a maximum. To confirm that $L^2(H_2O)RhOO^{2+}$ was indeed formed, as in eq 10, H_2O_2 (0.18−0.23 M) was added to reaction solutions immediately following completion of the reaction between $L^2(H_2O)RhOOH^{2+}$ (21−25 μM) and a slight excess of $Ru(bpy)_3^{3+}$ (24−28 μM). The addition of H_2O_2 caused the absorbance at 270 nm to decrease, signaling the consumption of $L^2(H_2O)RhOO^{2+}$, as was expected on the basis of the known[27] $H_2O_2/L^2(H_2O)RhOO^{2+}$ reaction ($k/s^{-1} = 4.60 \times 10^{-4} + 2.14 \times 10^{-3}$ $[H_2O_2]$).[27] The signal-to-noise ratio and the precision of the kinetic data were smaller owing to the large background absorption by $Ru(bpy)_3^{2+}$, but both the observed rate constants and absorbance changes were within 20% of those expected[27] for the $H_2O_2/L^2(H_2O)RhOO^{2+}$ reaction. This experiment confirms that the oxidation of $L^2(H_2O)RhOOH^{2+}$ with $Ru(bpy)_3^{3+}$ indeed takes place as in eq 10.

$$L^2(H_2O)RhOOH^{2+} + Ru(bpy)_3^{3+} \rightarrow L^2(H_2O)RhOO^{2+} + Ru(bpy)_3^{2+} + H^+ \quad (10)$$

An extremely slow reaction was observed between $L^2(H_2O)RhH^{2+}$ and $Ru(bpy)_3^{3+}$. From the initial rates, the

(26) Pestovsky, O.; Bakac, A. *J. Am. Chem. Soc.* **2003**, *125*, 14714–14715.

(27) Furczon, M.; Pestovsky, O.; Bakac, A. *Inorg. Chem.* **2007**, *46*, 11461–11466.

Table 3. Summary of Hydrogen Atom and Hydride Transfer Reactions of Rhodium Hydrides and Hydroperoxides

oxidant	hydrogen donor	k_{RhOOH}/ M^{-1} s^{-1}[a]	mechanism[b]	k_{RhH}/k_{RhOOH}[c]	source
$Ru(bpy)_3^{3+}$	$L^2(H_2O)RhOOH^{2+}$	4.7×10^4 [d]	ET	$<4 \times 10^{-6}$	this work
O_3	$(NH_3)_4(H_2O)RhOOH^{2+}$	6.9×10^3	HT	32	34
$(salen)Cr^VO^+$	$L^2(H_2O)RhOOH^{2+}$	1.2×10^3	HT	0.8	this work, 19
$Cr_{aq}OO^{2+}$	$(NH_3)_4(H_2O)RhOOH^{2+}$	46	HAT	2.9	18, 35
$Cr_{aq}OO^{2+}$	$L^1(H_2O)RhOOH^{2+}$	23	HAT	5.6	18, 35
$Cr_{aq}OO^{2+}$	$L^2(H_2O)RhOOH^{2+}$	17	HAT	1.4	18, 35
$Cr^{IV}{}_{aq}O^{2+}$	$(NH_3)_4(H_2O)RhOOH^{2+}$	$\sim 10^4$	HAT	~ 1[e]	18, 19

[a] In 0.10 M $HClO_4$. [b] HAT = hydrogen atom transfer; ET = electron transfer; HT = hydride transfer. [c] Ratio of the rate constants for rhodium(III) hydrido and hydroperoxo complexes with identical ligands. [d] In 1.0 M $HClO_4$. [e] Hydride data pertain to $L^1(H_2O)RhH^{2+}$.

observed rate constant is <0.4 M^{-1} s^{-1}. The slowness of the reaction combined with the kinetic instability of $Ru(bpy)_3^{3+}$ at longer times prevented us from using limiting $[L^2(H_2O)RhH^{2+}]$ to determine the stoichiometry. It is reasonable to assume that the reaction starts as a one-electron oxidation (eq 11), similar to that of other complexes in this work. The fate of the initial rhodium product, presumably $L^2(H_2O)RhH^{3+}$, is not known, but it is highly unlikely that the oxidized hydride would homolyze to Rh^{III} and the hydrogen atom in analogy to oxidized superoxo and nitrosyl complexes. The heterolysis to Rh^{II} and H^+ (eq 12) is energetically much more favorable and would seem to offer a more probable pathway. The $L^2(H_2O)Rh^{2+}$ generated in reaction 12 would be rapidly oxidized by $Ru(bpy)_3^{3+}$ (eq 9), leading to an overall stoichiometry of $[Ru(bpy)_3^{3+}]/[L^2(H_2O)RhH^{2+}] = 2$ and $k_{11} < 0.2$ M^{-1} s^{-1}.

$$Ru(bpy)_3^{3+} + L^2(H_2O)RhH^{2+} \rightarrow Ru(bpy)_3^{2+} + L^2(H_2O)RhH^{3+} \quad (11)$$

$$L^2(H_2O)RhH^{3+} \rightarrow L^2(H_2O)Rh^{2+} + H^+ \quad (12)$$

The reaction between $(salen)Cr^VO^+$ and $L^2(H_2O)RhOOH^{2+}$ was studied briefly to provide a comparison for the corresponding $L^2(H_2O)RhH^{2+}$ reaction studied previously.[19] A 1:1 stoichiometry was established from the absorbance changes with limiting $L^2(H_2O)RhOOH^{2+}$ (eq 14).

$$(salen)Cr^VO^+ + L^2(H_2O)RhOOH^{2+} \xrightarrow{H^+, H_2O} (salen)Cr^{III}(OH_2)_2^+ + L^2Rh(H_2O)_2^{3+} + O_2 \quad (13)$$

Kinetic determinations yielded the rate constants $k_{14} = 532$ M^{-1} s^{-1} (in 5.0 mM $HClO_4$), 695 M^{-1} s^{-1} (in 26 mM $HClO_4$), and 795 M^{-1} s^{-1} (in 30 mM $HClO_4$). There was no evidence for intermediates, suggesting a single-stage reaction, most likely hydride transfer. The dependence on $[HClO_4]$ is fully accounted for by the ionic strength (μ) effect on this reaction. The data were fitted to eq 14, where z_A and z_B represent charges on the reactants and $A = 0.509$ for aqueous solutions at 25 °C. The fit yielded the product ratio $z_Az_B = 1.9$, close to the expected value of 2.0. The rate constant listed in Table 3, $k_{13} = (1.20 \pm 0.10) \times 10^3$ M^{-1} s^{-1}, was obtained by extrapolation of the data fit to 0.10 M ionic strength.

$$\log k = \log k_0 + 2Az_Az_B\mu^{1/2}/(1 + \mu^{1/2}) \quad (14)$$

Discussion

Structurally, the new macrocyclic chromium nitrosyl complex $L^1(H_2O)CrNO^{2+}$ strongly resembles the aqua analogue [L = $(H_2O)_4$].[25,28] Similarly, the position of the first maximum in the visible spectrum is almost the same (449−452 nm) for all three complexes [L = $(H_2O)_4$, L^1, and L^2], and molar absorptivities at each maximum are all within a factor of 2. These data also suggest[13] similar electronic structures for all three complexes, with the $Cr^{III}-NO^-$ limit providing the closest description. As was already commented,[13,25] the limiting structures are only an approximation but one that is helpful in understanding and rationalizing the chemistry of these complexes.

The macrocyclic nitrosyl complexes are oxidized more slowly by $Ru(bpy)_3^{3+}$ than the aqua analogue is (Table 2). The same trend also holds for the superoxide complexes. Of the two series, the nitrosyl complexes are the less reactive, a fact that can be attributed, at least in part, to less favorable thermodynamics,[13] as shown below.

The driving force for dissociative oxidation can be calculated from reduction potentials for the $LM(H_2O)_2^{3+/2+}$ couples and binding constants K_{16}^{-1}, as illustrated for $Cr_{aq}OO^{2+}$ in eqs 15, 16a, and 17a and for $Cr_{aq}NO^{2+}$ in eqs 15, 16b, and 17b. The potential E_{17b} for $Cr_{aq}NO^{2+}$ will be more negative than −0.29 V obtained for the superoxo complex because NO binding to chromium is stronger,[29,30] and reaction 16b will have a more negative potential than reaction 16a does.

$$Cr_{aq}^{2+} - e^- \rightleftarrows Cr_{aq}^{3+} \quad 0.41\ V \quad (15)$$

$$Cr_{aq}OO^{2+} \rightleftarrows Cr_{aq}^{2+} + O_2 \quad -0.70\ V \quad (16a)$$

$$Cr_{aq}NO^{2+} \rightleftarrows Cr_{aq}^{2+} + NO \quad (16b)$$

(28) Levina, A.; Turner, P.; Lay, P. A. *Inorg. Chem.* **2003**, *42*, 5392–5398.
(29) The rate constant k_{-16b} for the Cr_{aq}^{2+}/NO reaction is greater[30] than k_{-16a} for the Cr_{aq}^{2+}/O_2 reaction. The dissociation (reaction 16a) is quite favorable for $Cr_{aq}OO^{2+}$, but reaction 16b is too slow to observe for $Cr_{aq}NO^{2+}$. Thus, the ratio $k_{-16}/k_{16} = K_{16}^{-1}$ must be much greater for $Cr_{aq}NO^{2+}$ than for $Cr_{aq}OO^{2+}$, even though the precise value of K_{16b}^{-1} is not known.
(30) Nemes, A.; Pestovsky, O.; Bakac, A. *J. Am. Chem. Soc.* **2002**, *124*, 421–427.

$$Cr_{aq}OO^{2+} - e^- \rightleftarrows Cr_{aq}{}^{3+} + O_2 \quad -0.29\ V \qquad (17a)$$

$$Cr_{aq}NO^{2+} - e^- \rightleftarrows Cr_{aq}{}^{3+} + NO \qquad (17b)$$

If the greater reactivity of aquachromium complexes in both the nitrosyl and superoxo series is indeed thermodynamic in origin, then the substantially more negative reduction potentials of $L(H_2O)_2Cr^{3+/2+}$ [31] relative to $Cr_{aq}{}^{3+/2+}$ would have to be more than offset by greater binding constants $K_{16a}{}^{-1}$ and $K_{16b}{}^{-1}$ for the macrocyclic complexes. The support for this hypothesis is currently limited by the lack of observable homolysis in all of the chromium macrocyclic complexes in Table 2. It is also apparent that the reactivity drop from aqua to L^1 and L^2 complexes is greater for the chromium superoxides than for the nitrosyls so that the gap between k_{MOO} and k_{MNO} becomes smaller. This result suggests that perhaps K_{17a} and K_{17b} for the chromium macrocycles are closer to each other than the corresponding values for the aquachromium analogues.

The slow oxidation of the superoxo rhodium complex $L^2(H_2O)RhOO^{2+}$ (Table 2) is qualitatively also consistent with the notion that the thermodynamic scheme in eqs 15−17 plays a role in the kinetics. The strongly endothermic potential for this reaction (equivalent of $E_{17a} = -0.81$ V) is a result of the low reducing power of $L^2Rh(H_2O)^{2+}$ ($E^0 = 0.13$ V)[27] and strong binding of O_2 to $L^2Rh(H_2O)^{2+}$ (equivalent of $K_{16a}{}^{-1} = 2.7 \times 10^{12}$ M^{-1}).[27] However, the difference in rate constants for the oxidation of $Cr_{aq}OO^{2+}$ (2630 M^{-1} s^{-1}) and $L^2(H_2O)RhOO^{2+}$ (15.8) (Table 2) is rather small for the >0.5 V difference in E_{17a} for the two reactions. Thermodynamics clearly have only a modest effect on the oxidation kinetics. This point is even more pronounced for the macrocyclic superoxo complexes. If the kinetics were dominated by thermodynamics, then the comparable rate constants k_{MOO} for $L^2(H_2O)RhOO^{2+}$ and $L^2(H_2O)CrOO^{2+}$ would require K_{17a} values to also be comparable. This, in turn, would require the binding constant $K_{16a}{}^{-1}$ for $L^2(H_2O)_2CrOO^{2+}$ to be extremely large (10^{24} M^{-1}) to undo the effect of the large negative reduction potential for $L^2Cr(H_2O)_2{}^{3+}$ (assumed to be comparable to that for the unmethylated analogue $L^1Cr(H_2O)_2{}^{3+}$, i.e., −0.64 V).[31] There is no obvious reason for the binding of O_2 to macrocyclic chromium complexes to be so exceptionally strong, suggesting that their smaller than expected reactivity must be nonthermodynamic in origin. The intrinsic reactivity of these complexes, as measured by self-exchange reactions, is unfortunately not known, but our results suggest that the self-exchange rate constants for the $L(H_2O)CrOO^{3+/2+}$ are greater than those for the rhodium analogues.

$L^2(H_2O)RhH^{2+}$ and $L^2(H_2O)RhOOH^{2+}$. The reduction potential for the couple {$L^2(H_2O)RhOO^{2+}$, $H^+/L^2(H_2O)$-$RhOOH^{2+}$} is 0.97 V.[32] That for {$L^2Rh(H_2O)^{2+}$, $H^+/L^2(H_2O)$-RhH^{2+}} is not known, but it is estimated to lie in the range of 0.5 ± 0.2 V based on a typical bond dissociation free energy for $L^2(H_2O)Rh-H^{2+} = 270 \pm 20$ kJ mol^{-1} and the reduction potential for the $H^+/H^{\bullet}$ couple (−2.29 V).[33] Thus, the hydride is by far the better reductant thermodynamically, but it reacts with $Ru(bpy)_3{}^{3+}$ much more slowly than the hydroperoxide. Qualitatively, this is the same pattern as that observed in HAT reactions,[18] but the relative reactivity of the hydride is even lower in the electron-transfer reaction with $Ru(bpy)_3{}^{3+}$.

The oxidation of hydrides with both ozone and $(salen)Cr^VO^+$ is believed to take place by hydride transfer.[34] The ozone reaction with the hydride $(NH_3)_4(H_2O)RhH^{2+}$ is faster than that with the corresponding hydroperoxide, whereas in the reactions with $(salen)Cr^VO^+$, the macrocyclic metal hydride and hydroperoxide exhibit comparable reactivity (Table 3). The hydroperoxide has a steric advantage in that the hydrogen to be abstracted is separated from the rhodium center by a peroxo bridge, which facilitates the approach by oxochromium to reach the transition state that we picture as $[(salen)Cr^VO\cdots H\cdots OORh(H_2O)L^2]$. In the reaction of rhodium hydride, the two metal centers are much closer, $[(salen)Cr^VO\cdots H\cdots Rh(H_2O)L^2]$. Atom transfer reactions involving macrocyclic rhodium complexes have been shown to be extremely slow if both reactants bear a saturated macrocycle.[35] In the $L^2(H_2O)RhH^{2+}/(salen)Cr^VO^+$ reaction, only one of the macrocycles is saturated while the other is nearly planar, but the required closeness of the approach still suggests severe steric interference. We suggest that the larger intrinsic reactivity of the hydride is diminished by steric effects, and the similarity in the rate constants for the hydride and hydroperoxide is coincidental. This argument does not apply to any of the remaining reactions in Table 3, all of which involve, at most, a single macrocyclic complex.

Our data suggest that the unusually slow reactions of rhodium(III) hydrides, observed in this work and earlier, are more prominent in one electron processes, i.e., HAT and electron transfer, but even in two-electron reactions in the absence of significant steric hindrance, such as in hydride transfer to ozone, the hydride complex is only marginally more reactive than the hydroperoxide.

The most striking difference between the two is found in outer-sphere electron transfer with $Ru(bpy)_3{}^{3+}$ (Table 3), where the ratio $k_{RhH}/k_{RhOOH} < 4 \times 10^{-6}$. Because steric effects should play a minimal role in outer-sphere electron transfer, it is clear that intrinsic reactivity of the hydride is much smaller and that hydride reactions benefit more by a change of mechanism to either HAT or hydride transfer. In the language of inorganic chemistry, the hydride reaction is facilitated by a bridged transition state (inner-sphere electron transfer) much more than the hydroperoxide.

Acknowledgment. We are grateful to Ms Sally Mcintyre and Dr. Sam Houk for help with ICP-MS experiments. This work was supported by a grant from the National Science Foundation (Grant CHE 0602183). Some of the work was conducted with the use of facilities at the Ames Laboratory.

Supporting Information Available: Plots of rate constants vs concentratrions (Figures S1 and S2). This material is available free of charge via the Internet at http://pubs.acs.org.

IC800867J

(31) Bakac, A.; Butkovic, V.; Espenson, J. H.; Orhanovic, M. *Inorg. Chem.* **1993**, *32*, 5886–5888.
(32) Szajna-Fuller, E.; Bakac, A. *Inorg. Chem.* **2007**, *46*, 10907–10912.
(33) Buxton, G. V.; Greenstock, C. L.; Helman, W. P.; Ross, A. B. *J. Phys. Chem. Ref. Data* **1988**, *17*, 513–886.
(34) Vasbinder, M.; Bakac, A. *Inorg. Chim. Acta* **2008**, *361*, 3193–3198.
(35) Bakac, A. *J. Am. Chem. Soc.* **1997**, *119*, 10726–10731.